JOURNAL OF GEOPHYSICAL RESEARCH: SPACE PHYSICS, VOL. 118, 6302–6318, doi:10.1002/jgra.50594, 2013

A new diffusion matrix for whistler mode chorus waves

Richard B. Horne,[1] Tobias Kersten,[1] Sarah A. Glauert,[1] Nigel P. Meredith,[1]
Daniel Boscher,[2] Angelica Sicard-Piet,[2] Richard M. Thorne,[3] and Wen Li[3]

Received 20 May 2013; revised 9 August 2013; accepted 23 September 2013; published 15 October 2013.

[1] Global models of the Van Allen radiation belts usually include resonant wave-particle interactions as a diffusion process, but there is a large uncertainty over the diffusion rates. Here we present a new diffusion matrix for whistler mode chorus waves that can be used in such models. Data from seven satellites are used to construct 3536 power spectra for upper and lower band chorus for $1.5 \leq L^* \leq 10$ MLT, magnetic latitude $0° \leq |\lambda_m| \leq 60°$ and five levels of K_p. Five density models are also constructed from the data. Gaussian functions are fitted to the spectra and capture typically 90% of the wave power. The frequency maxima of the power spectra vary with L^* and are typically lower than that used previously. Lower band chorus diffusion increases with geomagnetic activity and is largest between 21:00 and 12:00 MLT. Energy diffusion extends to a few megaelectron volts at large pitch angles > 60° and at high energies exceeds pitch angle diffusion at the loss cone. Most electron diffusion occurs close to the geomagnetic equator (< 12°). Pitch angle diffusion rates for lower band chorus increase with L^* and are significant at $L^* = 8$ even for low levels of geomagnetic activity, while upper band chorus is restricted to mainly $L^* < 6$. The combined drift and bounce averaged diffusion rates for upper and lower band chorus extend from a few kiloelectron volts near the loss cone up to several megaelectron volts at large pitch angles indicating loss at low energies and net acceleration at high energies.

Citation: Horne, R. B., T. Kersten, S. A. Glauert, N. P. Meredith, D. Boscher, A. Sicard-Piet, R. M. Thorne, and W. Li (2013), A new diffusion matrix for whistler mode chorus waves, *J. Geophys. Res. Space Physics*, *118*, 6302–6318, doi:10.1002/jgra.50594.

1. Introduction

[2] Whistler mode chorus waves are usually characterized by short duration bursts of radiation below the local electron gyrofrequency f_{ce} which rise or fall rapidly in frequency [*Burtis and Helliwell*, 1969; *Tsurutani and Smith*, 1974; *Tsurutani et al.*, 2013]. These bursts may only last a few milliseconds but they often overlap and occur repeatedly for many hours [*Santolík et al.*, 2003]. A chorus wave burst may reach amplitudes of 240 mV m^{-1} or more [*Cattell et al.*, 2008] at frequencies from a few hundred hertz to a few kilohertz outside the Earth's plasmapause. Chorus waves have also been observed inside the magnetospheres of Jupiter, Saturn, Uranus, Neptune, and the Jovian moon Ganymede [*Gurnett and Scarf*, 1983; *Gurnett et al.*, 1986; *Scarf et al.*, 1987; *Hospodarsky et al.*, 2008].

[3] Chorus waves can interact strongly with electrons over a wide energy range from a few hundred electron volts up to several megaelectron volts via Doppler shifted cyclotron resonance [*Horne and Thorne*, 2003]. These cyclotron resonant interactions result in pitch angle diffusion of electrons into the loss cone and, hence, due to the bursty nature of the waves, they have been associated with bursts of precipitation observed by balloons and satellites at low altitudes [*Rosenberg et al.*, 1971; *Imhof et al.*, 1992; *Lorentzen et al.*, 2001; *Saito et al.*, 2012; *Tsurutani et al.*, 2013] and the loss of electrons from the radiation belts into the atmosphere. Pitch angle scattering by chorus is also largely responsible for both the diffuse aurora [*Thorne et al.*, 2010; *Ni et al.*, 2011] and pulsating aurora [*Nishimura et al.*, 2010; *Miyoshi et al.*, 2010].

[4] Chorus waves can also cause substantial energy diffusion and acceleration of the trapped electron population [*Horne and Thorne*, 1998; *Summers et al.*, 1998; *Horne et al.*, 2005a, 2005b], particularly in regions of low plasma density [*Horne et al.*, 2003; *Meredith et al.*, 2002]. It is now suggested that these waves play a major role in the formation of the outer radiation belt at Earth [*Horne*, 2007] as they cause electron acceleration inside geostationary orbit. Similarly, chorus waves can accelerate electrons up to a few megaelectron volts at Jupiter where it has been suggested that they provide the missing step in a chain of processes that starts with volcanic activity on the Moon Io and ends with synchrotron radiation from the planet near $1.6R_j$ [*Horne et al.*, 2008].

[1] British Antarctic Survey, Cambridge, UK.
[2] French Aerospace Laboratory, Toulouse, France.
[3] Department of Atmospheric and Oceanic Sciences, University of California, Los Angeles, California, USA.

Corresponding author: R. B. Horne, British Antarctic Survey, Natural Environment Research Council, Madingley Road, Cambridge CB3 0ET, UK. (R.Horne@bas.ac.uk)

2169-9380/13/10.1002/jgra.50594

[5] At the Earth, chorus is usually observed outside the plasmapause from about 22:00 MLT through dawn to the dayside [*Meredith et al.*, 2001, 2012; *Li et al.*, 2009, 2011]. Typically, the waves are observed most often near dawn extending from the plasmapause to beyond $L = 7$. Observations show that chorus is most intense during substorms [*Meredith et al.*, 2001] and is related to plasma injections by convective and inductive electric fields [*Lyons et al.*, 2005]. Typically, the amplitude of chorus takes 5 h to decay at geostationary orbit following a substorm [*Meredith et al.*, 2000]. Under special conditions, chorus can propagate along the magnetic field and reach the ground. Ground-based observations at Halley Research Station, Antarctica also show that chorus is associated with substorms [*Smith et al.*, 2004a, 2004b] and that the intensity of chorus is highest near dawn, consistent with the injection and transport of 1–10 keV electrons. Furthermore, observations show that chorus wave intensities can remain high between midnight and dawn for several days following magnetic storms [*Smith et al.*, 2004a, 2004b] and during high speed solar wind stream events with predominantly southward IMF B_z [*Lyons et al.*, 2005; *Miyoshi et al.*, 2007; *Li et al.*, 2012].

[6] Observations show that the Poynting flux of chorus waves is away from the magnetic equator [*Santolík et al.*, 2010], strongly suggesting that these waves are generated very close to the magnetic equator. Typically, observations show that wave power is highest at latitudes of just a few degrees above and below the magnetic equator. The frequency-time characteristics and discrete bursty nature of the signals suggests that the waves are generated by nonlinear wave-particle interactions, and several theories have been proposed [*Trakhtengerts*, 1999; *Nunn et al.*, 1997; *Omura et al.*, 2007, 2009]. The general concept is that plasma injected toward the Earth during substorms forms a temperature anisotropy which causes linear wave growth at frequencies $\omega/\Omega_e \leq A/(1 + A)$ where A is the temperature anisotropy given by $A = T_\perp/T_\parallel - 1$, and $T_\perp$ ($T_\parallel$) is the electron temperature perpendicular (parallel) to the direction of the Earth's magnetic field [*Kennel and Petschek*, 1966]. According to nonlinear theory, the waves cause phase trapping of electrons which then act as a resonant current. As the waves propagate along the magnetic field, the phase trapped electrons re-radiate at a higher (lower) frequency with a nonlinear growth rate [*Nunn*, 1974; *Omura et al.*, 1991, 2009; *Katoh and Omura*, 2007]. A key aspect of the theory is the spatial gradient of the magnetic field, wave amplitude, and other inhomogeneities which determine whether rising or falling frequency elements are produced [*Nunn et al.*, 2009]. Test particle simulations for a plasma with a large temperature anisotropy and dipole magnetic field show that rising frequency chorus elements can be produced from a broad band of waves representing a background of plasmaspheric hiss [*Omura et al.*, 2009; *Katoh and Omura*, 2007, 2011], and simulations using a one-dimensional Vlasov Hybrid simulation code can replicate both rising and the rarer falling tone chorus [*Nunn et al.*, 2009]. Test particle simulations also show that, with a sufficiently long wave packet of the order of one second, seed electrons with energies of the order several hundred kiloelectron volts can be accelerated to megaelectron volt energies through a nonlinear trapping process called relativistic turning acceleration [*Omura et al.*, 2007; *Furuya et al.*, 2008].

[7] While the generation of chorus waves takes place on a timescale of a few milliseconds, the waves may be observed repeatedly over a period of several days during geomagnetic storms. On this timescale it is not possible to use fully nonlinear theory to determine the impact of the waves on the electron population due to the computational effort required and so some approximation must be used. One of the most often used approximations is quasi-linear theory. In this approach the wave power of the discrete chorus elements is averaged over space and time and electron phase trapping is omitted. This enables the impact of the waves on the electron distribution to be treated as a diffusion problem [*Schulz and Lanzerotti*, 1974], which can be applied on a global scale. It is difficult to assess whether quasi-linear modeling underestimates or overestimates the acceleration of electrons when compared with the nonlinear approach, particularly since the nonlinear approach depends on whether chorus elements are rising or falling in frequency, their amplitude, how often they repeat, and also depends on the field gradient which changes with local time and geomagnetic activity. However, using quasi-linear theory, several studies have shown the importance of chorus for electron acceleration and loss and how they control the dynamics of the outer radiation belt [*Varotsou et al.*, 2005, 2008; *Albert et al.*, 2009; *Shprits et al.*,2009a, 2009b; *Fok et al.*, 2008; *Su et al.*, 2010]. The quasi-linear diffusion approach is now also used in physical models to forecast the Earth's radiation belts [*Horne et al.*, 2013].

[8] The accuracy and performance of global radiation belt models depends on the quality of the diffusion coefficients. Until now most models have used diffusion coefficients calculated from a model of the wave power spectra derived from CRRES satellite data [e.g., *Varotsou et al.*, 2005, 2008; *Li et al.*, 2007; *Albert et al.*, 2009; *Shprits et al.*, 2009b]. While these models have provided a very good first analysis, they are constructed from a data set that is very sparse on the dayside of the Earth near noon MLT and is limited in latitude and sampling at high levels of geomagnetic activity. The purpose of this paper is to present a new chorus diffusion matrix consisting of both bounce averaged and bounce and drift averaged diffusion rates in pitch angle, energy, and mixed pitch angle-energy that can be used in global radiation belt models. The diffusion rates are calculated from a numerical fit to power spectra obtained from seven different satellites for $1.5 \leq L^* \leq 10$, which greatly extend the coverage at large L^* particularly on the dayside. The diffusion matrix has 3 h resolution in MLT, extends the previous range of latitudes from 0°–30° to 0°–60°, and provides diffusion rates for five instead of three levels of geomagnetic activity.

2. Chorus Wave Database

[9] The diffusion matrix was constructed from wave data observed by seven different spacecraft, Dynamics Explorer 1 (DE 1), the Combined Release and Radiation Effects Satellite (CRRES), Cluster 1, Double Star TC1, and the Time History of Events and Macroscale Interactions during Substorms (THEMIS A, D, and E). Each satellite has different frequency bands, only a subset of which overlap in frequency. To combine the data from different satellites, the wave magnetic field data were first integrated over frequency to obtain the wave intensity in nT^2 and quality controlled

Table 1. Frequency Bands Grouped Into Upper and Lower Band Chorus and Normalized to the Local Value of f_{ce}

Lower Band Chorus	Upper Band Chorus
0.0117–0.02333	0.5–0.6
0.02333–0.1	0.6–0.7
0.1–0.2	0.7–0.8
0.2–0.3	0.8–0.9
0.3–0.4	0.9–1.0
0.4–0.5	

to remove spurious data. Only the wave electric field data were available from CRRES, but this was converted into wave magnetic field by assuming field-aligned propagation of the waves and the appropriate electron density, as done in previous work [e.g., *Meredith et al.*, 2003]. Since chorus waves are often observed as lower band chorus below $0.5f_{ce}$ and upper band chorus between 0.5 and $1.0f_{ce}$ [e.g., *Tsurutani and Smith*, 1974], the data were then separated into 11 frequency bands which were scaled according to the local f_{ce} as given in Table 1. The data were then transformed into the L^* coordinate system using the ONERA DESP library v4.2 [*Boscher et al.*, 2008] since this later enables the bounce and drift averaged diffusion rates to be calculated for a given drift path. The conversion into L^* was performed using the IGRF field model at the middle of the appropriate year and the Olson-Pfitzer quiet magnetic field model [*Olson and Pfitzer*, 1977] as recommended by the COSPAR Panel for Radiation Belt Environment Modeling. The resulting wave database contains the wave intensity in nT^2. More details on data collection, quality control, identification of chorus waves, conversion into L^* coordinates, and analysis of these data are described in detail elsewhere [*Meredith et al.*, 2012].

[10] To form the diffusion matrix, the wave data were separated into 18 equally spaced bins in L^* between $L^*_{\min}$ = 1.5 and $L^*_{\max}$ = 10, with ΔL^* = 0.5, 10 bins in latitude, 6° wide, between 0° and 60°, eight bins in MLT, 3 h wide, and five levels of K_p ($K_p < 1$, $1 \leq K_p < 2$, $2 \leq K_p < 3$, $3 \leq K_p < 4$, and $K_p > 4$). Thus, there are 7200 bins with 11 different frequency bands. The frequency bands were grouped into two bands for upper and lower band chorus making 14,400 data bins. However, when wave power and data quality were taken into account, the actual number of fitted spectra were much lower than this, as described below.

[11] The data were split into five levels of geomagnetic activity based on K_p rather than AE so that the diffusion matrix can be used in space weather forecasting models to forecast the radiation belt flux [e.g., *Horne et al.*, 2013]. These models use a forecast of the K_p index to set the diffusion coefficients and hence produce the forecast. In reality, chorus waves are associated with substorms and are better organized by AE, but while forecasts of K_p are routinely available there is no method of forecasting AE reliably at present.

3. Models for f_{pe}/f_{ce}

[12] In order to calculate the diffusion rates the ratio f_{pe}/f_{ce} is required in each data bin for the five levels of geomagnetic activity. This effectively means developing five plasma density models. We took the approach of using observations where possible. Plasma density measurements were obtained from the wave instrument on CRRES and inferred from measurements of the spacecraft potential and electron thermal speed on THEMIS [*Li et al.*, 2010] and were converted to L^* and then binned into the same L^* bins as described above, but for 1 h MLT resolution instead of 3 h. The data were combined for a latitude range of $-9° < \lambda_m < 9°$ to provide better data coverage. Data at higher latitudes were not included so as to minimize any latitude effects. Plasma density measurements were not easily available for the other spacecraft and were not used to construct the density models.

[13] Since chorus waves are mainly observed outside the plasmapause but plasmaspheric hiss inside the plasmapause can be confused with chorus when observed with low time resolution wave instruments, some method of identifying when the spacecraft were outside the plasmapause was required. For CRRES, we used the previously established observation that electron cyclotron harmonic (ECH) waves between $1 < f/f_{ce} < 2$ are only observed outside the plasmapause and applied the ECH criterion used in previous studies [*Meredith et al.*, 2004], namely that if the ECH wave electric field amplitude between $1 < f/f_{ce} < 2$ was greater than 0.0005 mV m^{-1}, then the satellite was deemed to be outside the plasmapause. For THEMIS the plasmapause was taken as the location where the total electron density $N_c = 5 \times 10^7$ m^{-3} for $L^* > 4.4$ and $N_c = 10(6.6/L^*)^4$ for $L^* < 4.4$ [*Li et al.*,2010]. Figure 1 (top row) shows the data for the five levels of K_p. As K_p increases note that f_{pe}/f_{ce} tends to decrease near dawn for $L^* < 6$ and less data is available at large L^* on the dayside.

[14] Nearer to the Earth, for $K_p < 1$, there are less data in the afternoon MLT sector but the data coverage tends to move closer to the Earth as K_p increases. This is consistent with the observed shape of the plasmapause which extends to large L^* in the afternoon and the exclusion of chorus waves in this region via the ECH criterion. However, the data extend closer to the Earth than one might expect, especially for low K_p. Typically, under quiet conditions, the plasmapause may lie near L^* = 4 and extend to larger L^* in the afternoon sector. This suggests that using the ECH criterion to define locations outside the plasmapause is not perfect, and some events may have been classified incorrectly. However, the diffusion coefficients are directly proportional to the wave intensity which is very low at low L^*, and thus any errors in the density or the boundary at low L^* are unlikely to cause any significant errors in the diffusion rates. The alternative is to use a plasma density model [e.g., *Carpenter and Anderson*, 1992]. However, such models are based on data from fewer satellites than we have used here and have limited information on the location of the plasmapause for different levels of geomagnetic activity. We have therefore chosen to base our calculations on the observed data where available rather than use a model.

[15] Between $L^*_{\min}$ and $L^*_{\max}$, f_{pe}/f_{ce} was interpolated to fill in any missing data bins. The interpolation was done in a number of steps for each level of K_p. On the dayside the largest L^* for which there were data in at least 8 MLT bins was determined (without missing data in two adjacent bins), and then missing data were linearly interpolated using nearest neighbor values and weighted by the number of samples. This was repeated on the nightside. The matrix was then completed by linear extrapolation to larger L^* to form the

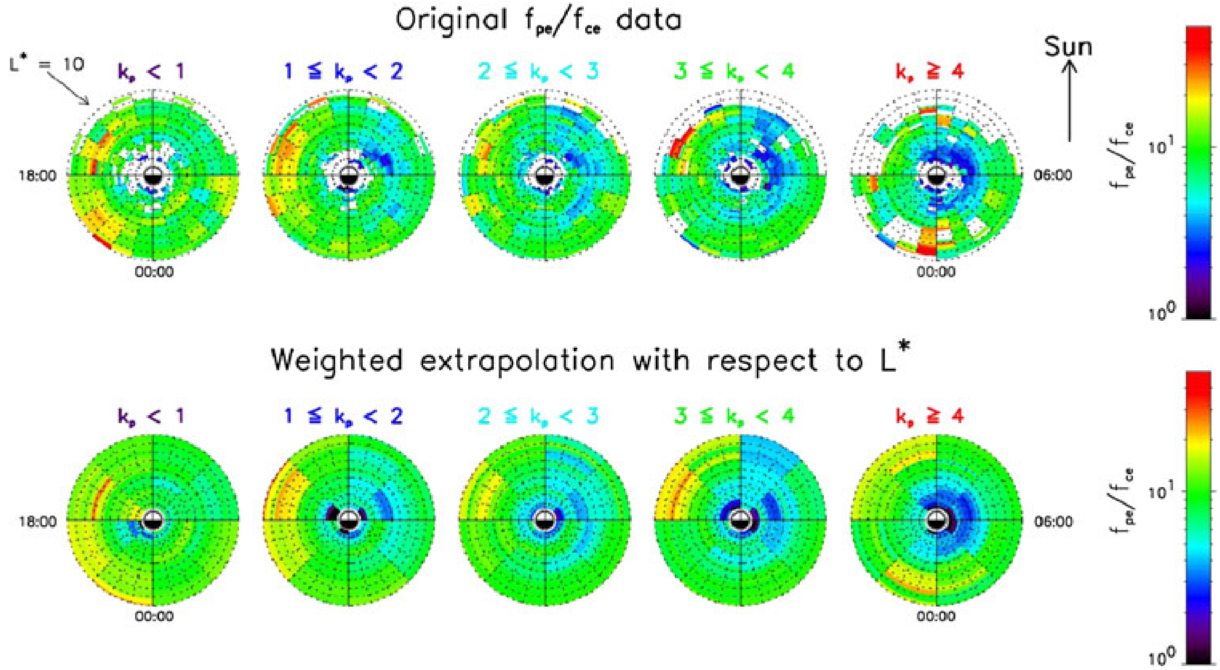

Figure 1. (top row) The f_{pe}/f_{ce} for five levels of K_p for $|\lambda_m| < 9°$ from satellite data. (bottom row) The f_{pe}/f_{ce} after interpolation and used in the model.

values of f_{pe}/f_{ce} in the equatorial plane, and averaged over 3 h of MLT. At higher latitudes, f_{pe}/f_{ce} was recalculated using a dipole magnetic field for all latitudes $0° \leq \lambda_m \leq 60°$. Figure 1 (bottom row) shows the model results. One of the noticeable features for $K_p > 4$ is that some values of f_{pe}/f_{ce} are very high just before midnight at large L^*. Inspection shows that there were relatively few samples in this location and that they correspond to very low values of f_{ce}, probably due to field line stretching during active periods. Rather than ignore these events, we have included them. Note also that the lowest values of f_{pe}/f_{ce} occur for typically $L^* < 6$ near dawn for higher levels of K_p, which is one of the most favorable conditions for chorus wave acceleration [*Horne et al.*, 2003].

[16] Although plasma density measurements from the other five spacecraft were not easily available, it was still necessary to determine when these spacecraft were outside the plasmapause. This was done using the model of *Carpenter and Anderson* [1992].

4. Fitting the Power Spectra

[17] In order to calculate the bounce averaged pitch angle $\langle D_{\alpha\alpha}\rangle$, energy $\langle D_{EE}\rangle$, and mixed $\langle D_{\alpha E}\rangle$ diffusion rates, the PADIE diffusion code [*Glauert and Horne*, 2005] requires the power spectral density to have a Gaussian form given by

$$B^2(\omega) = A^2 \exp\left(-\left(\frac{\omega-\omega_m}{\delta\omega}\right)^2\right) \quad (1)$$

where

$$A^2 = \frac{|B_w|^2}{\delta\omega}\frac{2}{\sqrt{\pi}}\left[\mathrm{erf}\left(\frac{\omega_m-\omega_{lc}}{\delta\omega}\right)+\mathrm{erf}\left(\frac{\omega_{uc}-\omega_m}{\delta\omega}\right)\right]^{-1} \quad (2)$$

where B_w is the wave amplitude in Tesla, ω_m is the (angular) frequency of the maximum in the power spectrum, $\delta\omega$ is the width of the power spectrum, ω_{lc} (ω_{uc}) is the lower (upper) frequency cutoff. These characteristic frequencies and wave intensity were obtained by fitting the data to Gaussian functions, as described below. As chorus often appears in two bands separated by a gap in frequency near $0.5f_{ce}$ [*Tsurutani and Smith*, 1974], the 11 frequency bands in the wave database were grouped into $f < 0.5f_{ce}$ for lower band chorus (six bands) and $0.5 < f/f_{ce} < 1$ for upper band chorus (five bands), as given in Table 1. Upper and lower band chorus were then fitted separately.

[18] The data provided from the wave database are in the form of $B^2(f)$ and not $B^2(\omega)$. However, since $\int B^2(\omega)d\omega = |B_w|^2 = \int B^2(f)df\, B^2(f)$ can be written in exactly the same form as equations (1) and (2) with ω replaced with f. A Gaussian function was fitted to the data using a nonlinear least squares fitting procedure called MPFIT [*Markwardt*, 2009] which was remarkably robust. The procedure was used to obtain f_m, δf, and a constant A_f^2 analogous to (2) and hence determine B_w.

[19] Since the diffusion coefficients are directly proportional to the power spectral density (PSD), there is no point in trying to fit very weak signals. However, if a threshold is set on the power spectral density, this may capture narrow signals but omit weak signals spread over a much wider frequency band and which could have a significant contribution. To capture both, the PSD was integrated over the lower (upper) chorus frequency band to obtain B_w. Since the diffusion rates are proportional to B_w^2, and B_w varies up to 100 pT or more for lower band chorus, and 20 pT or more for upper band chorus, fits were only performed if the measured wave intensity $B_w > 1$ pT.

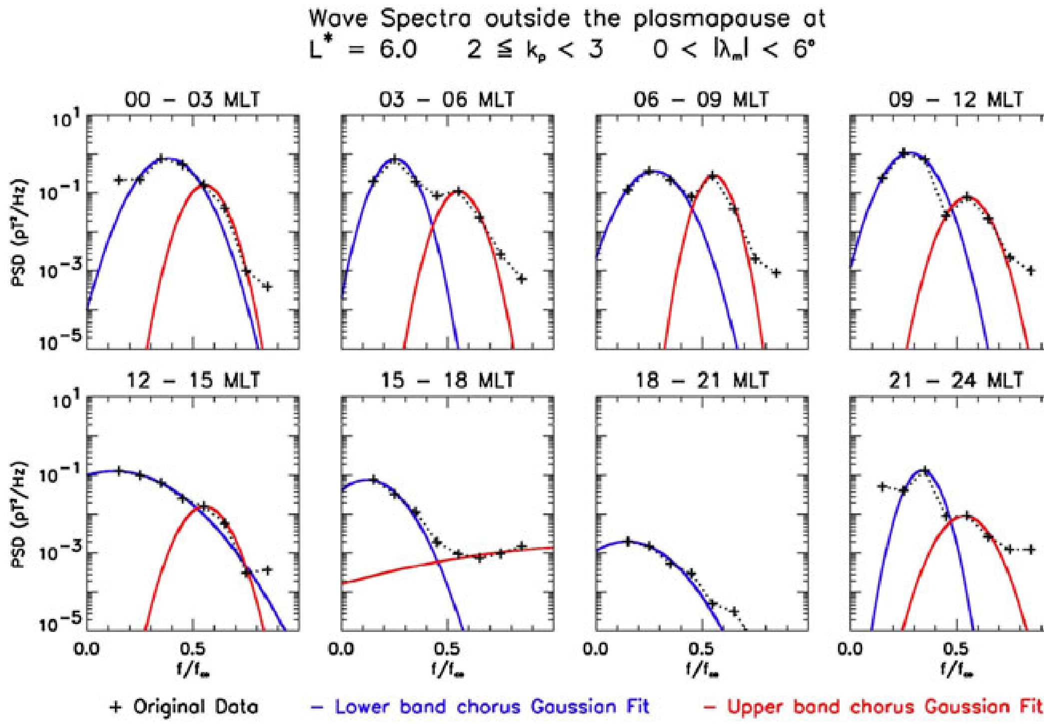

Figure 2. Comparison between the observed (dotted) and fitted (solid) power spectra for upper (red) and lower (blue) band chorus waves for eight MLT sectors, $|\lambda_m| < 6°$, $L^* = 6.0$, and $2 \le K_p < 3$.

[20] For each individual spectral profile, we performed five nonlinear least squares fits using five different step sizes for the numerical derivatives. The "goodness" of the fit was quantified using the Pearson χ^2 parameter where the best fit has a value closest to zero. In each case we selected the fit with the lowest value of χ^2. In general, better fits were found when the data exhibited a Gaussian shape, but in a number of cases, there appeared to be more than one peak in the lower band chorus spectra, mainly at low L^* and very large L^*. The second peak mostly appeared below $0.1f_{ce}$. When two peaks were present in the data, the resultant Gaussian fit would often result in a very narrow spectrum with more wave power at the lowest frequencies which was unlikely to be chorus. This was most undesirable as it would mean higher-electron diffusion at higher energies which was not due to chorus waves. Given the very large amount of data that had to be fitted, and the difficulties in trying to fit more than one power spectrum inside each band, it was decided to fit one Gaussian power spectrum in each band. Since strong chorus is not generally expected below $0.1f_{ce}$, and at low L^*, this is more likely to be plasmaspheric hiss or magnetosonic waves when close to the magnetic equator, data below $0.1f_{ce}$ were omitted for lower band chorus. When these data were removed, the fitting improved significantly.

[21] If some of the wave power below $0.1f_{ce}$ does correspond to chorus, then the consequences of omitting the two lowest frequency channels are that the diffusion rates for high-energy electrons would be underestimated resulting in a reduced electron acceleration rate and an underestimate of the electron loss rate at high, typically MeV energies. The investigation of low frequency waves is potentially very important and warrants more study, but this is outside the scope of the present paper.

[22] Upper band chorus data also revealed an occasional second peak at the highest frequency $0.95f_{ce}$. Usually, upper band chorus is observed at frequencies below $0.7f_{ce}$ and so the presence of wave power near $0.9f_{ce}$ is unexpected. This could be a result of the finite bandwidth of the CRRES PWE and Cluster Whisper frequency channels where wave power corresponding to other wave modes such as electron cyclotron harmonic waves above f_{ce} is translated into wave power just below due to binning the data. For this reason, the highest frequency data point in this frequency band was omitted and the quality of the fit improved significantly.

[23] It is unlikely that wave power near $0.9f_{ce}$ is due to chorus, particularly since waves near the harmonic resonances should be strongly damped. If it were, the consequences are that electron diffusion at very low energies would be underestimated, typically in the few tens to hundred electron volt range. This is well below the energy range for the radiation belts (typically > 100 keV) and the omission is unlikely to affect the results significantly.

[24] Figure 2 shows an example of the fitted power spectra for different MLT, $|\lambda_m| < 6°$, $L^* = 6.0$, and $2 \le K_p < 3$. Double-banded chorus with clearly distinguished peaks is most evident between 03:00 and 12:00 MLT. Note also that in some cases, the best fit to the data is provided by a very broad Gaussian spread, for example, for upper band chorus between 15:00 and 18:00 MLT. When calculating the diffusion rates, wave power is restricted to the appropriate frequency range by the upper and lower frequency cutoffs f_{uc} and f_{lc}, discussed below.

[25] Table 2 shows a summary of the statistics for fitting upper and lower band chorus. Out of a possible 14,400 data bins, 2738 spectra were fitted for lower band chorus and 798 for upper band chorus. There were only 22 cases

Table 2. Summary Statistics for Fitting Chorus Wave Spectra

	Lower Band				Upper Band			
Latitude	No Data	< 1 pT	No Fit	Fits	No Data	< 1 pT	No Fit	Fits
0°–6°	156	22	1	541	175	204	3	338
6°–12°	171	24	3	522	182	292	1	245
12°–18°	197	29	4	490	203	403	2	112
18°–24°	237	47	2	434	239	420	0	61
24°–30°	271	78	0	371	278	416	3	23
30°–36°	320	175	0	225	341	373	1	5
36°–42°	342	283	0	95	360	360	0	0
42°–48°	419	263	0	38	446	273	0	1
48°–54°	515	199	0	6	518	193	1	8
54°–60°	570	133	1	16	575	140	0	5
Total				2738				798

where the fit was not acceptable, otherwise there was either a lack of data or the wave amplitude was below the threshold.

5. Evaluation of the Fitting

[26] Figure 3 (top row) shows the wave intensity B_w^2 for lower band chorus obtained from the fit to the data for $|\lambda_m| < 6°$. Chorus wave intensities increase with increasing K_p, particularly from night through dawn to the dayside, consistent with previous observations [*Meredith et al.*, 2012]. The data also show that chorus can become particularly intense for increasing L^* near dawn, out to $L^* = 9$. Figure 3 (bottom row) shows the ratio of B_w^2 from the fit to that obtained from the data by integrating the PSD between 0.1 and $0.5 f_{ce}$. The results show that the fits capture more than 80% of the wave intensity, and typically more than 90%.

[27] Figure 4 (top row) shows the corresponding results for upper band chorus. Strong upper band wave intensities tend to be limited to $L^* < 6$, consistent with previous observations [*Meredith et al.*, 2012; *Li et al.*, 2011]. Again, Figure 4 (bottom row) shows that the fits to the data capture more than 90% of the wave intensity.

[28] Figure 5 provides examples of the other parameters derived from the fits to lower band chorus for low latitudes $|\lambda_m| < 6°$ and the region between 03:00 and 06:00 MLT where lower band chorus is strong. At low K_p, lower band chorus wave amplitudes only increase above the noise level

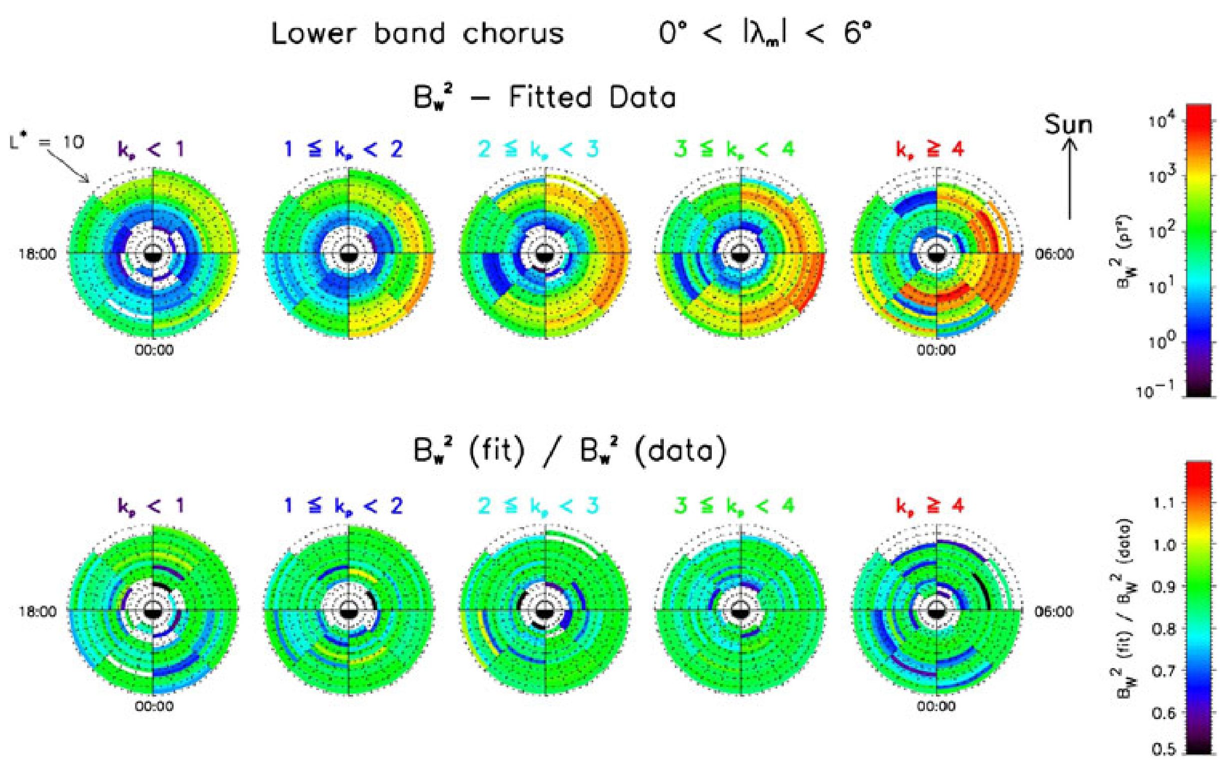

Figure 3. (top row) Wave intensity B_w^2 for lower band chorus obtained from the fits to the data and (bottom row) the ratio of the fitted B_w^2 to that obtained by integrating the power spectral density between $0.1 f_{ce}$ and $0.5 f_{ce}$ for $|\lambda_m| < 6°$.

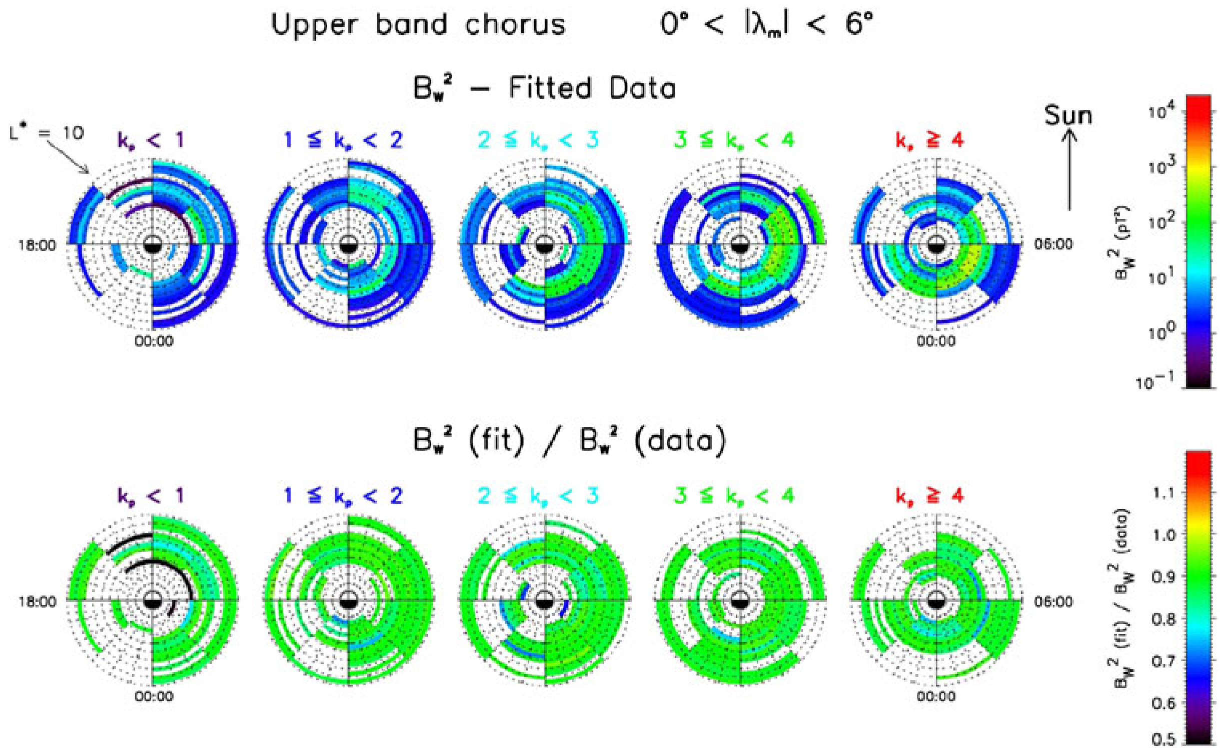

Figure 4. Same as Figure 3 but for upper band chorus.

for $L^* > 7$. Thus, as stated above, even if the waves at low L^* are not outside the plasmapause, their contribution to pitch angle and energy diffusion is very small. As K_p increases, chorus wave amplitudes increase and are observed at lower L^*. During very large magnetic storms, such as the 2003 geomagnetic storm, the plasmapause was confined to within $L < 2$ [*Baker et al.*, 2004], and thus, it is not surprising to see significant chorus amplitudes at $L^* = 3$ for high levels of geomagnetic activity.

[29] Figure 5 (second row) shows that where the wave amplitudes are significant, typically greater than 5 pT, f_m/f_{ce} tends to decrease with increasing L^*. In general, they range from 0.4 near $L^* = 3$ to 0.2 for $L^* > 8$. In contrast, the width of the power spectrum (Figure 5, third row) remains almost constant with L^*. The existing diffusion rates used in several global radiation belt studies [e.g., *Albert et al.*, 2009; *Fok et al.*, 2008; *Varotsou et al.*, 2005, 2008; *Shprits et al.*, 2009b] use a model where the relative frequency f_m/f_{ce} is fixed at 0.35 [*Glauert and Horne*, 2005]. Lower frequencies suggest more diffusion of higher-energy electrons, and from the data here suggest that this should become more important at larger L^*.

[30] The results for upper band chorus (Figure 6) show a different behavior to lower band chorus. As K_p increases, upper band chorus wave amplitudes increase and are observed at lower L^*, but they are restricted to $L^* < 6$. The reason why they are confined to $L^* < 6$ is not clear. Also, where $B_w > 5$ pT f_m/f_{ce} tends to remain almost constant with L^* and with K_p, at approximately $f_m/f_{ce} = 0.55$. Again, the width of the power spectrum (Figure 5, third row) is also approximately constant except at large L^* where wave amplitudes are small. Some of the peaks in $\delta f/f_{ce}$ correspond to small f_m/f_{ce} and are a consequence of fitting one Gaussian spectrum to data that may have more than one peak, as discussed above.

6. Wave Normal Angle

[31] In order to calculate the pitch angle and energy diffusion rates, a model for how the wave normal angle ψ varies with latitude is required. Here the wave normal angle is the angle between the k vector of the waves and the direction of the ambient magnetic field. The wave normal angle is important since it controls the number of cyclotron resonant interactions between the electrons and the waves. For parallel propagation along the magnetic field ($\psi = 0$), only the $n = -1$ cyclotron resonance is important, but as ψ increases, the Landau ($n = 0$) and higher harmonic resonances $n = \pm1, \pm2, \pm3, ...$ must be included in the calculation of the diffusion coefficients. Also, the wave normal angle changes the electron resonant energy, and hence the energy over which the particles are diffused.

[32] In general, the direction of the group velocity for whistler mode waves does not lie in the same direction as the phase velocity, or k vector of the waves. This is due to the anisotropic nature of magnetized plasma. Ray tracing shows that, to a first approximation, waves tend to propagate along the magnetic field when launched in the field-aligned direction at the magnetic equator in a dipole field. As they propagate to higher latitudes, the wave normal angle increases with latitude due to refraction mainly by the magnetic field gradient and can increase from 0° to 30° after propagating only 10° in latitude [e.g., *Horne and Thorne*, 2003, Figure 2] and continue increasing up to the resonance cone angle at higher latitudes. Although ray tracing provides a basis for how the wave normal angle varies with

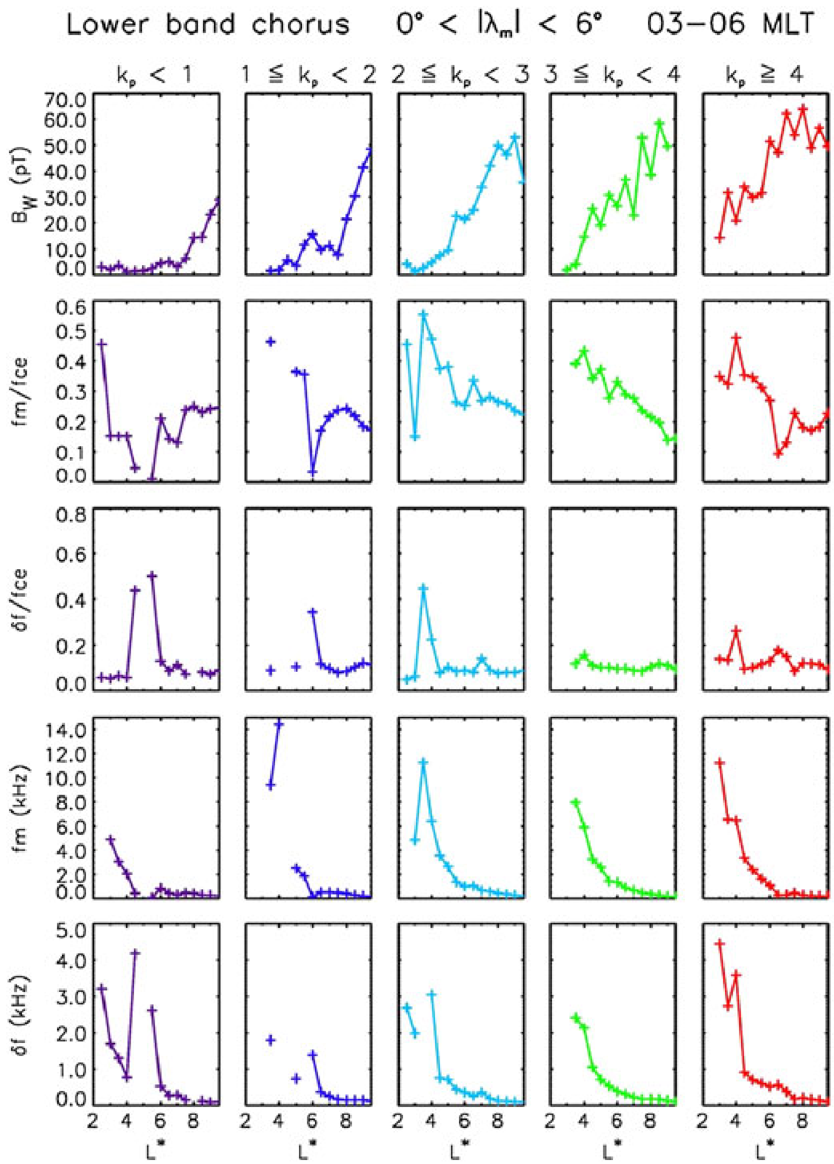

Figure 5. Parameters derived from fitting the power spectra for lower band chorus as a function of L^* for different levels of K_p, $0° < |\lambda_m| < 6°$, and 03:00–06:00 MLT. The parameters are the wave amplitude B_w, frequency of the maximum in the fitted power spectrum to the electron gyrofrequency f_m/f_{ce}, relative width of the power spectrum $\delta f/f_{ce}$, f_m, and δf.

latitude, observations reveal a more complex and sometimes conflicting behavior.

[33] For example, some of the earliest observations from OGO 5 and GEOS 2 found that the wave normal angles for lower band chorus were field aligned within a cone of angles less than 20° near the equator and became more oblique with increasing latitude [*Burton and Holzer*, 1974; *Hayakawa et al.*, 1984; *Goldstein and Tsurutani*, 1984]. However, several case events revealed larger angles, ψ = 30°–45°, close to the resonance cone [*Hayakawa et al.*, 1984]. For upper band chorus, ψ was close to the resonance cone, typically up to about 50°. Since these data were taken very close to the geomagnetic equator, they are expected to be close to the source region for chorus generation. Subsequent analysis of more case studies from GEOS 1 revealed that at a latitude of 17° there were two peaks in the wave normal angle distribution, typically near 45° and close to the resonance cone angle [*Muto et al.*, 1987]. However, at higher latitudes of 26°, the peak in the wave normal angle distribution, while still at a large angle, was typically 15°–20° less than the resonance cone angle [*Muto et al.*, 1987]. Other analysis shows that the wave normal angle distribution can vary significantly between 5° and 50° over a period of 0.5 s near L = 3.7 [*Lauben et al.*, 2002].

[34] More recent analysis of data from the POLAR satellite, which covered higher latitudes between 10° and 50° for L =3–7 shows that the highest probability of occurrence is for wave normal angles typically less than 42° [*Haque et al.*, 2010]. Furthermore, the wave normal angle distribution became narrower at higher latitude, typically 0°–10°. This is in complete contrast to ray tracing results and to observations by Cluster as it crossed the magnetic

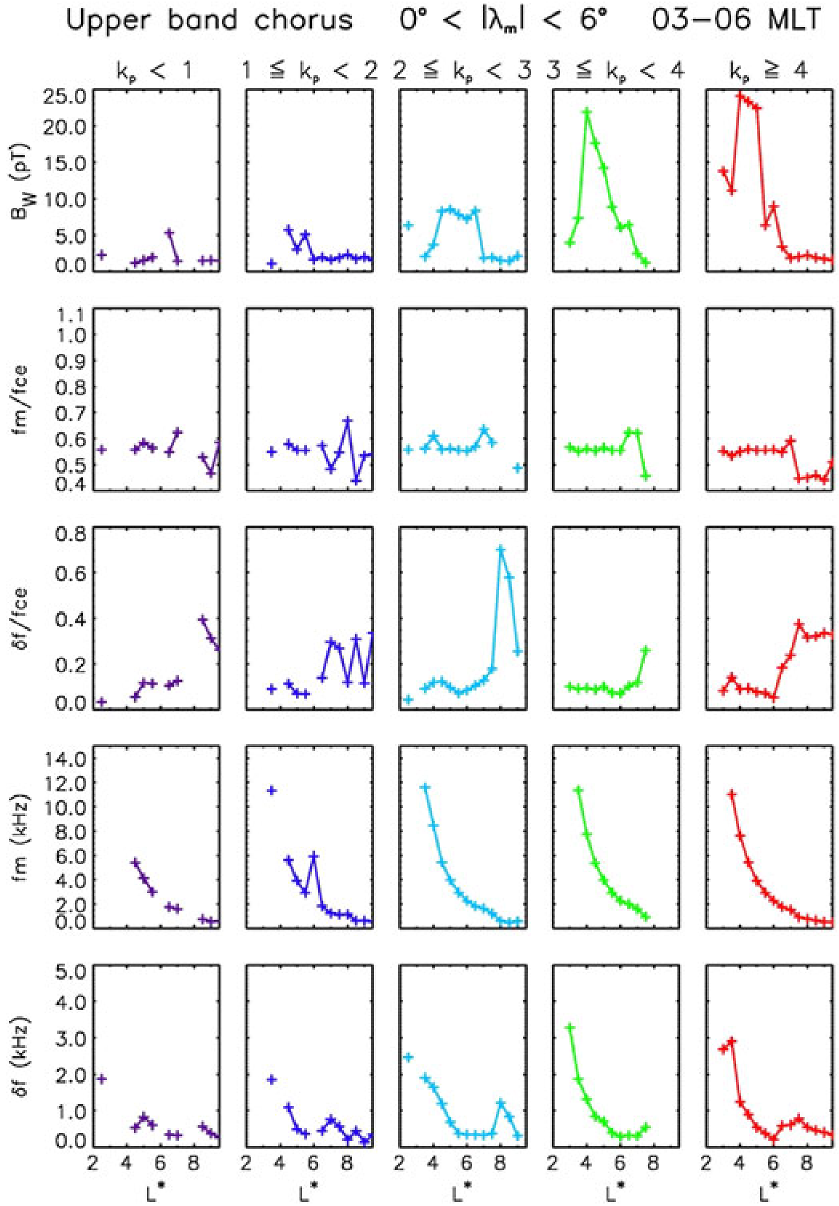

Figure 6. Same as Figure 5 but for upper band chorus.

equator near L = 4.5, which identified lower band chorus as almost exactly field aligned within 5° of the equator and then became more oblique with increasing latitude [*Santolík et al.*, 2003]. Analysis of 50 other events observed by Cluster [*Breneman et al.*, 2009] shows a peak near 20° and a second peak near 50° for lower band chorus, and a peak near 30° for upper band chorus. Other statistical analysis for Cluster shows that the wave normal angle for lower band chorus is small between 0° and 30°, but there can be another component at higher latitudes close to the resonance cone [*Agapitov et al.*, 2013].

[35] It is clear that there is no consensus yet on the distribution of wave normal angles for chorus waves. Some are field aligned even to high latitudes and some are field aligned near the equator and more oblique at higher latitudes. This behavior may be linked to the nonlinear generation of chorus as well as propagation effects. To calculate the diffusion rates using the PADIE code [*Glauert and Horne*, 2005], the distribution of wave normal angles is assumed to have a Gaussian form given by

$$g(X) = \exp\left(-\left(\frac{X - X_m}{X_w}\right)^2\right) \tag{3}$$

where $X = \tan\psi$, X_m corresponds to the maximum in the distribution and X_w is the width. For the purposes of this study, we have adopted a model based on a statistical analysis from THEMIS [*Li et al.*, 2011] and which agrees with the lower band chorus observations from Cluster for latitudes up to 30° [*Agapitov et al.*, 2013]. These studies show that the highest occurrence rate for lower band chorus waves for $|\lambda_m| < 5°$ is between ψ = 0° and 10° and increases slightly at higher latitudes to 0°–15°, but has a distribution that extends to 30° or so. The distribution tends to be more peaked in the

Table 3. Wave Parameters Used to Calculate the Diffusion Coefficients

Type of Wave	Spectral Properties	Angular Distribution	$X = \tan\psi$
Lower band chorus	f_m = fit δf = fit $f_{lc} = 0.1 f_{ce}$ $f_{uc} = 0.5 f_{ce}$	$\psi = 0°$ $\delta\psi = 30°$	$X_m = 0$ $X_w = 0.577$ $X_{lc} = 0$ $X_{uc} = 1.15$
Upper band chorus	f_m = fit δf = fit $f_{lc} = 0.5 f_{ce}$ $f_{uc} = 0.65 f_{ce}$	$\psi = 0°$ $\delta\psi = 30°$	$X_m = 0$ $X_w = 0.577$ $X_{lc} = 0$ $X_{uc} = 1.0$

field-aligned direction on the dayside than the nightside. THEMIS results also show that the highest occurrence rate for higher-amplitude waves is also $\psi = 0°–10°$. Thus, we have adopted a model in which the peak of the wave normal angle is field aligned ($X_m = 0$) and has a width $\delta\psi = 30°$ or $X_w = 0.577$ and retains this distribution with latitude and all MLT.

[36] Sample runs using the PADIE diffusion code showed that when the angular distribution of wave intensity was applied to the waves according to the wave normal angle distribution, some of the wave intensity could appear at angles that exceed the resonance cone angle at the higher frequencies. This is not allowed. Therefore, some method of restricting the wave intensity to angles less than the resonance cone angle is required. This is not straightforward since as the resonance cone is approached and the refractive index becomes large, whistler mode waves acquire a large quasi-electrostatic component. The wave magnetic field must be specified such that when the wave magnetic field is converted back to the wave electric field using Maxwell's equations, the quasi-electrostatic component must not become unrealistically large. Therefore, to prevent this we solved the dispersion relation and scaled down the wave magnetic field intensity according to the ratio of the square of the wave electric field component transverse to k, which is the electromagnetic component, to the square of the total wave electric field. Thus, it is possible that there is an electrostatic component to the wave diffusion which is not included here. Details of this procedure will be reported elsewhere. In reality, the wave power near the resonance cone is probably limited by electron Landau damping as the phase velocity becomes small, but this is outside the scope of the work here. Table 3 gives a summary of the parameters used to calculate the diffusion coefficients, including the upper and lower cut-offs (X_{uc}, X_{lc}) in the angular distribution and the upper frequency cut-off of $0.65 f_{ce}$ which is the same as that used in previous work [*Ni et al.*, 2011].

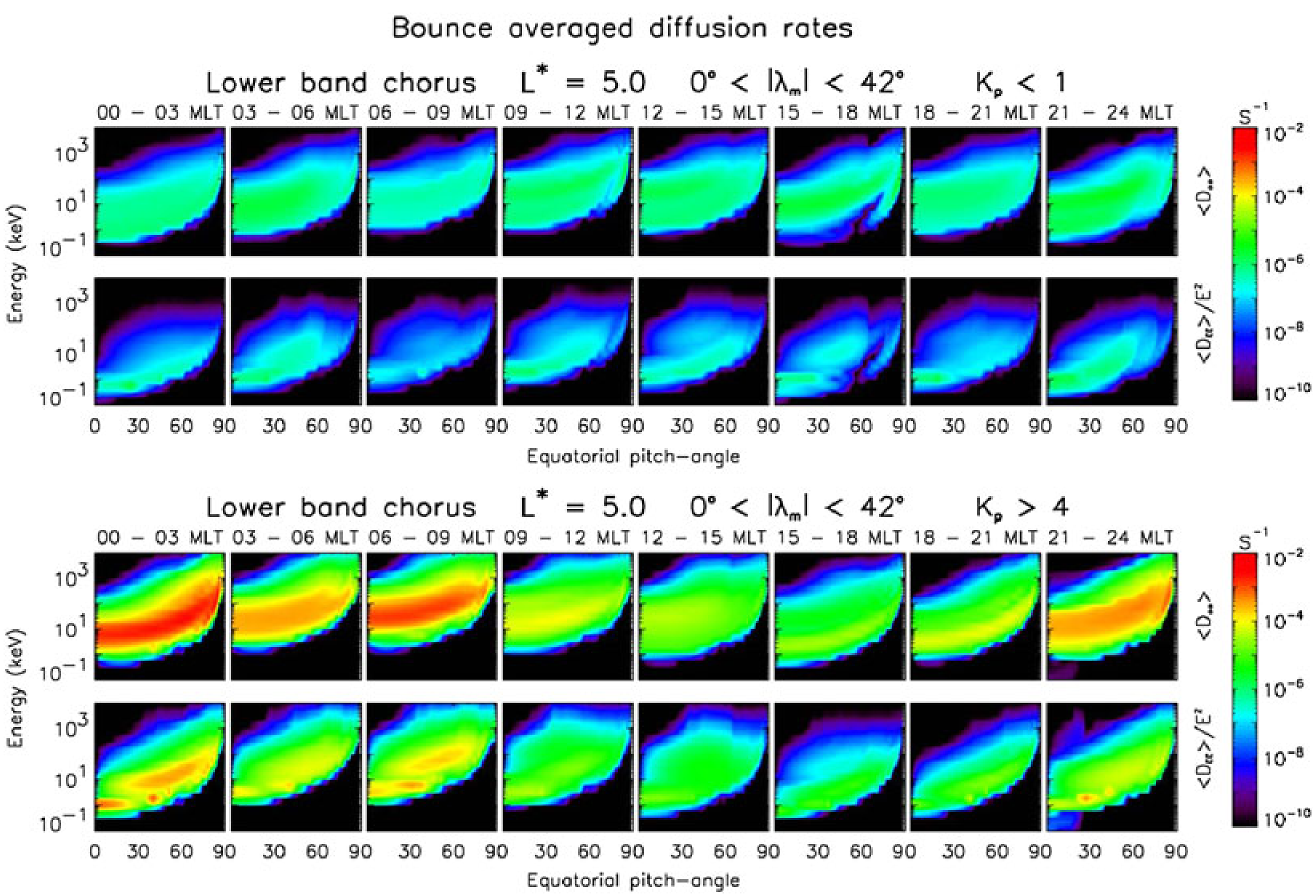

Figure 7. Bounce averaged pitch angle ($\langle D_{\alpha\alpha}\rangle$) and energy ($\langle D_{EE}\rangle/E^2$) diffusion rates for lower band chorus at $L^* = 5$, color coded as a function of energy and equatorial pitch angle α and for MLT increasing left to right. The top (bottom) two rows are for $K_p < 1$ ($K_p > 4$).

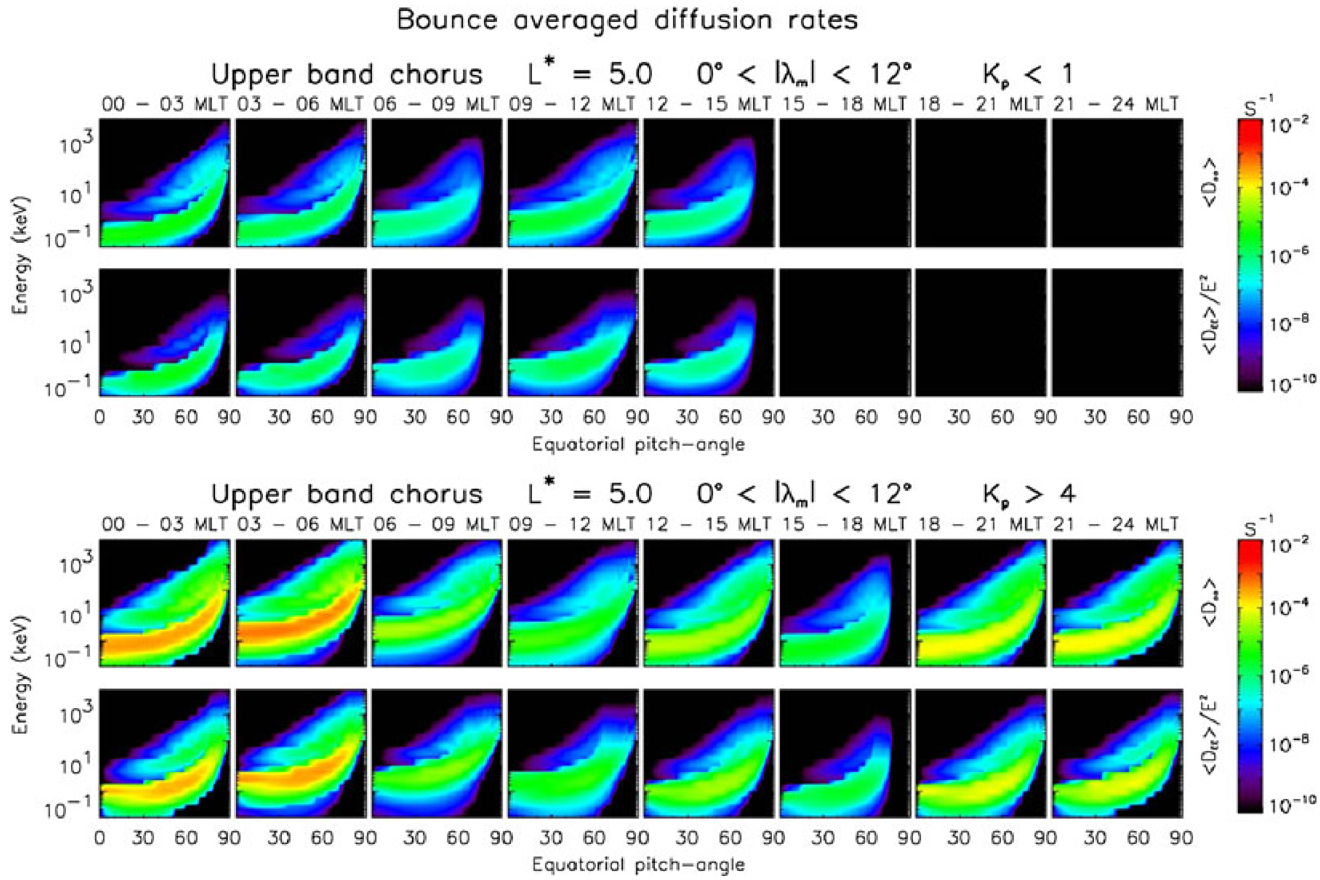

Figure 8. Same as Figure 7 but for upper band chorus.

7. Bounce Averaged Diffusion Rates

[37] In previous publications the diffusion coefficients have been defined in a number of different ways. In order to help make the correct comparisons, we define the bounce averaged diffusion coefficients as follows: for pitch angle $\langle D_{\alpha\alpha}\rangle = \langle\Delta\alpha\Delta\alpha/(2\Delta t)\rangle$; for mixed pitch angle energy $\langle D_{\alpha E}\rangle = \langle\Delta\alpha\Delta E/(2\Delta t)\rangle$; and for energy as $\langle D_{EE}\rangle = \langle\Delta E\Delta E/(2\Delta t)\rangle$. Thus, to compare the diffusion rates in units of s^{-1}, we must compare $\langle D_{\alpha\alpha}\rangle$, $\langle D_{\alpha E}\rangle/E$, and $\langle D_{EE}\rangle/E^2$. So, for example, $\langle D_{\alpha\alpha}\rangle$ here corresponds to $\langle D_{\alpha\alpha}\rangle/p^2$ in *Glauert and Horne* [2005].

[38] Using the PADIE code [*Glauert and Horne*, 2005] $\langle D_{\alpha\alpha}\rangle$, $\langle D_{EE}\rangle$, and $\langle D_{\alpha E}\rangle$ were calculated for each spectra for upper and lower band chorus, at energies of 100 eV, 200 eV, 300 eV, 600 eV, 1 keV, 2 keV, ... , 10 MeV, or 21 energy levels in total. Taking into account the total number of fits in Table 2, this amounted to $21 \times 3536 = 74,256$ runs of the PADIE code. Each run included the dominant resonances from $n = -5....5$ with a pitch angle resolution of 1°. Bounce averaging was done in each 6° latitude bin where the variation in the magnetic field was taken into account assuming a dipole magnetic field. The full bounce averaged diffusion rates for a given L^* were then computed by adding the diffusion rates for all latitude bins at the same L^*. Analysis showed that most of the wave intensity for lower (upper) band chorus was restricted to latitudes < 42° (< 12°) and so the diffusion coefficients were calculated up to these latitudes.

[39] The bounce averaged diffusion rates provide a measure of particle diffusion in pitch angle and energy, but a full understanding of how the waves change the distribution function and hence electron flux requires knowledge of the gradients in the distribution function as well and source and loss processes. Even so, the diffusion rates provide a very good indicator. Figure 7 provides an example for lower band chorus at $L^* = 5$ and two levels of K_p. During quiet periods, pitch angle diffusion is relatively weak and at small pitch angles near the loss cone extends over an energy range of typically 1–100 keV (Figure 7, top row). The region of pitch angle diffusion tends to increase in energy with increasing pitch angle extending up to about 1 MeV by 60° or so. The diffusion rates are significantly higher for $K_p > 4$ (Figure 7, bottom row) mainly from the premidnight sector through dawn to the dayside, between 21:00 and 09:00 MLT. This reflects the increased chorus wave power during active periods.

[40] At night, energy diffusion at $L^* = 5$ is significantly enhanced during active periods and has a peak close to the loss cone at an energy of approximately 1 keV. The direction of net particle diffusion depends on the gradient of the distribution function, but according to existing theory, energy diffusion is related to wave growth as electrons are diffused into the loss cone. Energy diffusion also peaks at higher energies of $\sim$ 10 keV and extends up to MeV energies at large pitch angles typically > 60°. Note that at the higher energies, energy diffusion at large pitch angles is higher

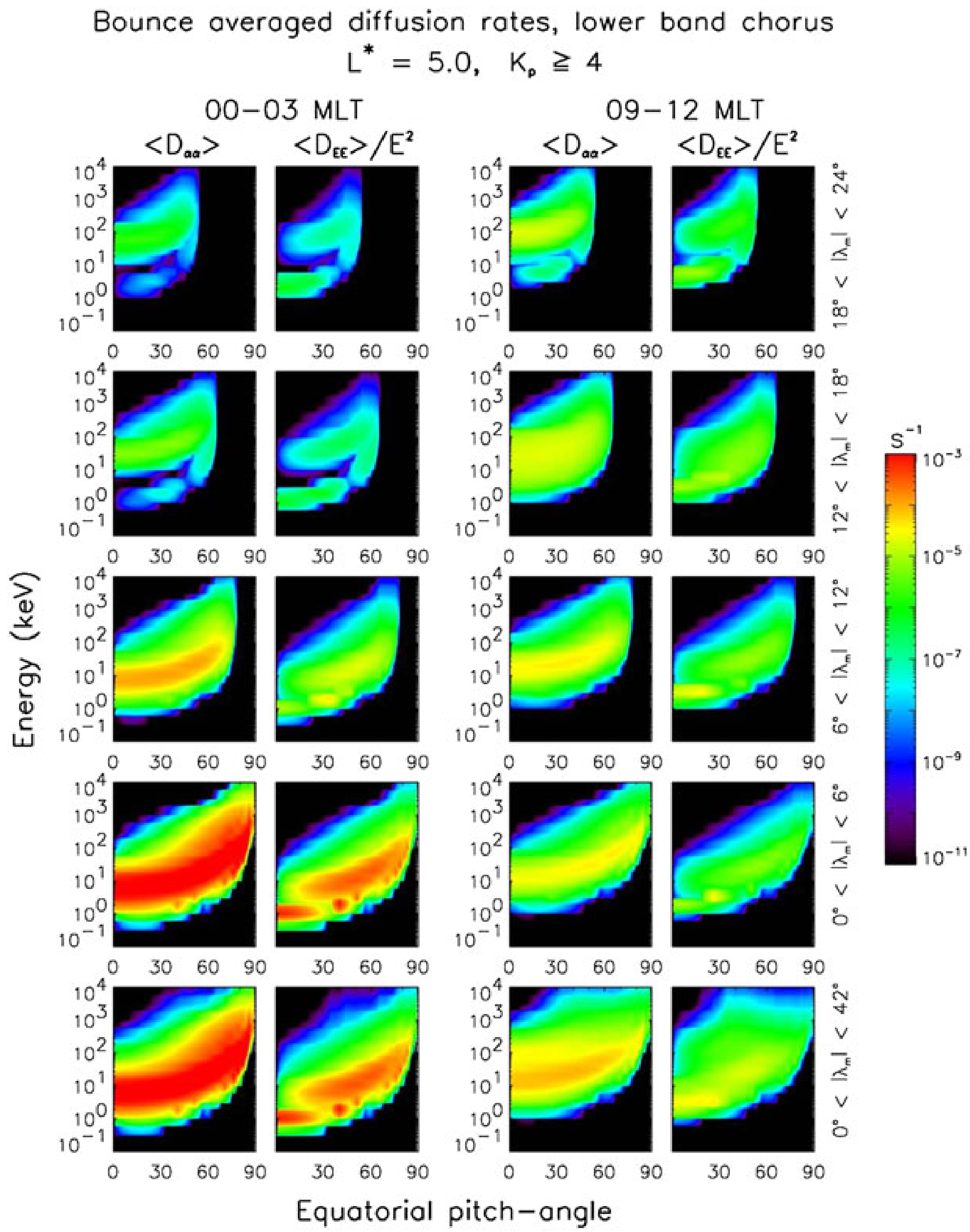

Figure 9. Bounce averaged pitch angle ($\langle D_{\alpha\alpha}\rangle$) and energy ($\langle D_{EE}\rangle/E^2$) diffusion rates for lower band chorus at $L^* = 5$ and $K_p \geq 4$, color coded as a function of energy and equatorial pitch angle α and for a range of different latitudes. The left (right) two columns are for 00:00–03:00 MLT (09:00–12:00 MLT). The bottom row is for the whole latitude range 0° < $|\lambda_m|$ < 6° while the other rows and for latitudes increasing bottom to top.

than pitch angle diffusion near the loss cone indicating that electrons can be accelerated without significant loss.

[41] Figure 8 shows an example for upper band chorus where wave intensity is above the threshold (1 pT^2). In this case the higher frequencies result in diffusion at much lower energies, typically a few hundred eV up to a few keV or so near the loss cone, but diffusion extends up to MeV energies at larger pitch angles. Again, at energies of 10 keV or more energy diffusion rates at large pitch angles exceed pitch angle diffusion rates at the loss cone.

[42] To determine how the latitude distribution of waves contributes to the diffusion rates, Figure 9 shows the bounce averaged diffusion rates for five different latitude ranges at two different MLT sectors corresponding to strong chorus wave amplitudes. The results show that the dominant contribution comes from waves near the magnetic equator for $|\lambda_m| < 6°$. The contribution from waves at higher latitudes is restricted to smaller equatorial pitch angles and suggests that energy diffusion to large pitch angles must take place near the equator. Energy diffusion near the loss cone at $\sim$ 1 keV is also predominantly a feature of the waves near the equator. It is interesting to note that while the peak in energy diffusion near the loss cone is near 1 keV, the peak in pitch angle diffusion is at higher energies of 10 keV. More

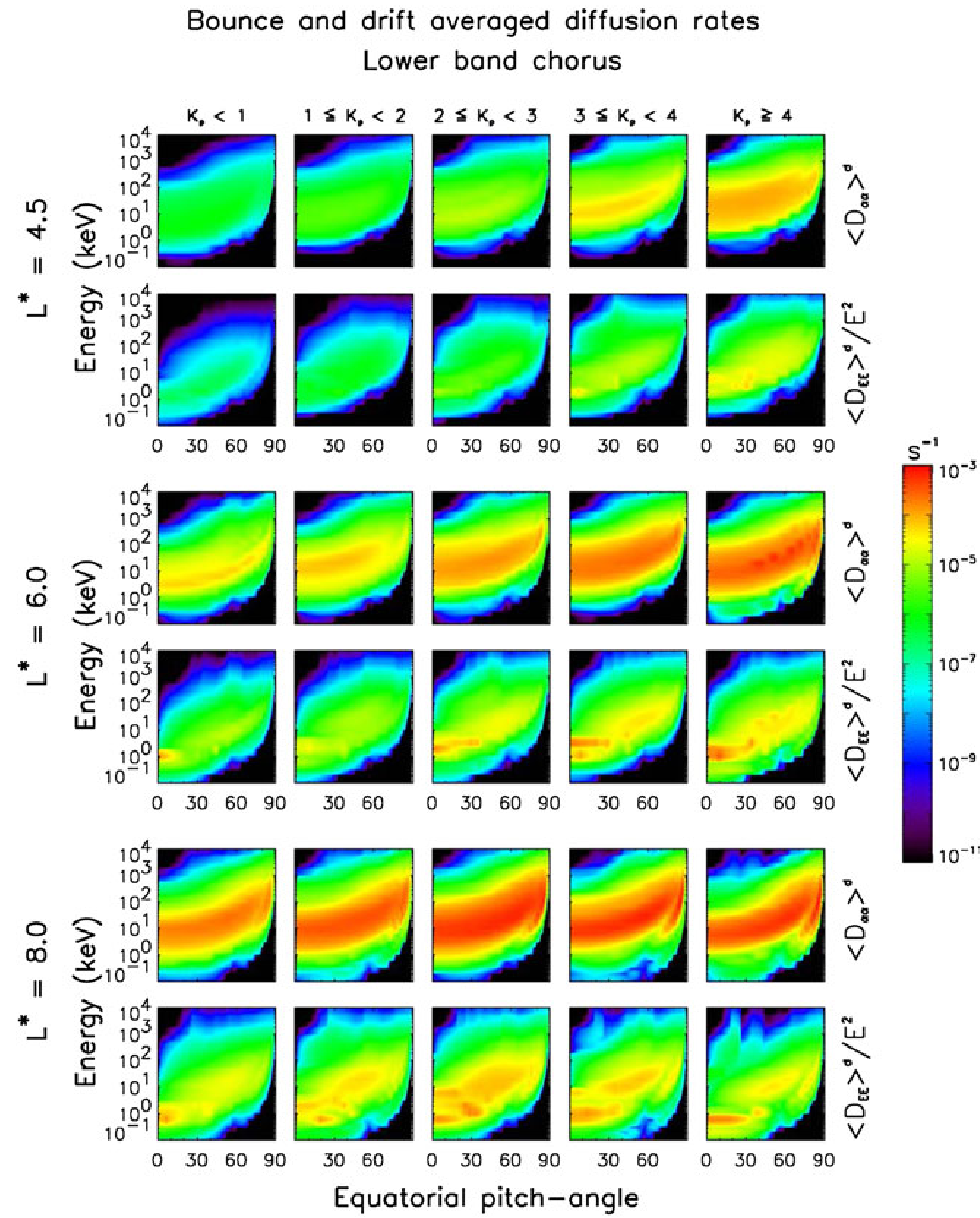

Figure 10. Bounce and drift averaged pitch angle ($\langle D_{\alpha\alpha}\rangle^d$) and energy ($\langle D_{EE}\rangle^d/E^2$) diffusion rates for lower band chorus, color coded as a function of energy and equatorial pitch angle for K_p increasing left to right and three values of L^*.

generally, diffusion rates at higher latitudes are stronger on the dayside than they are on the nightside. This reflects the observation that chorus wave power tends to be stronger at high latitudes on the dayside, and could be associated with a possible source at higher latitudes on the dayside [*Tsurutani and Smith*, 1977].

8. Drift and Bounce Averaged Diffusion Rates

[43] While a few models such as the Salammbô and RAM model include MLT resolution [*Jordanova et al.*, 2010], most models assume some form of drift average over MLT. We have therefore computed the drift and bounce averaged diffusion rates by adding the bounce averaged diffusion coefficients for each MLT bin and dividing by the number of bins, which is eight. For large values of K_p, it is likely that the magnetopause lies inside $L^* = 10$ [e.g., *Shue et al.*, 1997, 1998] and radiation belt electrons may be on open drift paths and experience losses at the magnetopause. The calculation and use of diffusion rates at large L^* must be considered carefully. Figure 3 shows that for $K_p \geq 4$, there is very little data for $L^* > 8$ near noon and the wave power

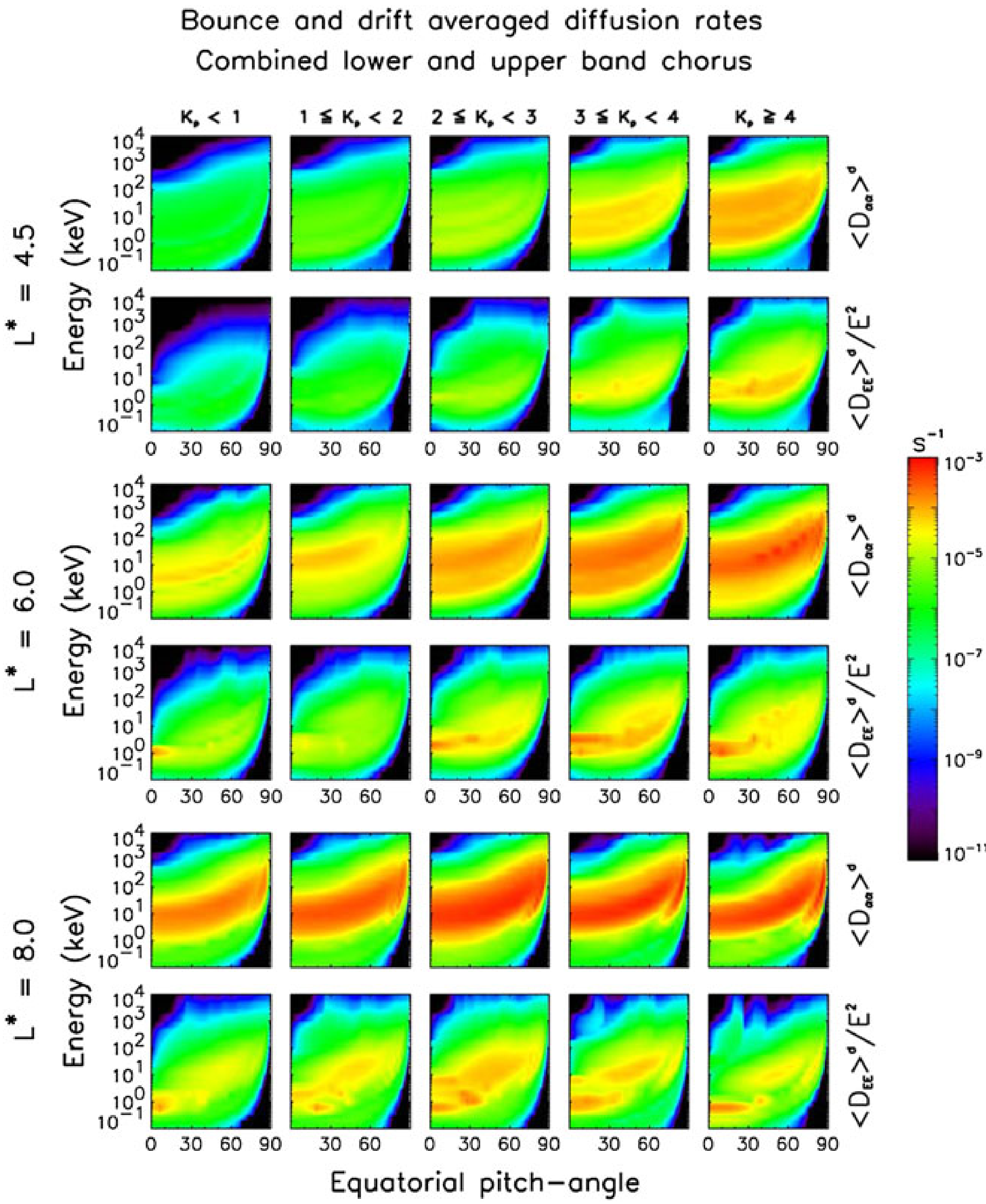

Figure 11. Same as Figure 10 but for upper and lower band chorus added together.

at larger L^* is zero. Thus, the effects of the magnetopause location on the waves are at least partially included. In each case we have divided the diffusion rates by the total number of bins in MLT (eight) and not just the number with nonzero data so that the diffusion rates are more likely to be an underestimate.

[44] Figure 10 shows the results for lower band chorus for three selected values of L^* and the five levels of K_p. While both pitch angle and energy diffusion increase with K_p, perhaps the most striking feature is that, for $K_p < 4$, the diffusion rates tend to increase with L^*. Even during relatively quiet magnetic activity ($K_p < 1$), pitch angle diffusion at $L^* = 8$ is larger than that at $L^* = 6$. For higher levels of K_p, the diffusion rates at $L^* = 6$ and 8 are comparable and may be larger near $L^* = 6$. This is an interesting feature as the peak in the electron phase space density is usually between $L^* =4$ and 6 during active times [*Green and Kivelson*, 2004; *Chen et al.*, 2007], which suggests that local acceleration and wave acceleration are the leading candidates. However, the results here also suggest that the role of radial diffusion and transport must also be taken into account very carefully. We also note that energy diffusion near the loss cone near 1 keV remains very significant.

[45] When upper and lower band chorus diffusion rates are combined (Figure 11), there is significant energy diffusion at $L^* = 4.5$ and large K_p from $\sim$ 0.1 to > 100 keV. At $L^* = 6$, there are two maxima in the pitch angle diffusion rates which are most apparent at small pitch angles due to the combination of upper and lower band chorus. Furthermore, pitch angle diffusion at $\sim$ 1 keV extends to much larger pitch

angles up to about 80°. This enables electrons to be diffused into the loss cone over a wide range of angles except near 90°. This type of structure in the diffusion rates has been shown to result in energy-dependent structure in the pitch angle distribution and the formation of pancake distributions [*Thorne et al.*, 2010; *Tao et al.*, 2011]. For L^* > 6, the diffusion rates are dominated by lower band chorus as large upper band chorus wave intensities are restricted to L^* < 6.

9. Summary and Conclusions

[46] Here we present a new diffusion matrix for upper and lower band chorus waves based on the analysis of wave and plasma data from seven different satellites and quasi-linear theory. The data extend the coverage of previous satellites particularly at large L^* between 7 and 10, extend the range of latitudes from 0°–30° to 0°–60°, provide more coverage in magnetic local time, particularly on the dayside, and more data for different levels of geomagnetic activity. The satellite data have been used to construct five plasma density models corresponding to five different levels of geomagnetic activity as measured by the K_p index, and 3536 fitted power spectra for upper and lower band chorus over a range of L^* between 1.5 and 10 with a resolution of $0.5L^*$, magnetic latitudes between 0° and 60° with a resolution of 6°, and all MLT with a 3 h resolution. The wave spectra have been carefully fitted using Gaussian functions to determine the frequency maxima, widths, and wave amplitudes needed to compute the diffusion coefficients. The fitting process captures typically more than 90% of the observed wave intensities. Fits to the data show that frequency maximum for lower band chorus typically decreases with increasing L^* from $0.4f_{ce}$ to $0.2f_{ce}$ and is generally lower than that used ($0.35f_{ce}$) in previous studies of the radiation belts. Lower band chorus wave amplitudes vary with MLT and K_p up to typically a few hundred pT. The PADIE code was used to calculate the bounce averaged pitch angle, energy, and mixed pitch angle-energy diffusion coefficients for each power spectra where data are available for B_w > 1 pT. Combining the diffusion rates along a given L^*, this gives a bounce averaged chorus diffusion matrix of $3 \times 1440 = 4320$ coefficients and a drift and bounce averaged diffusion matrix of 540 coefficients as a function of equatorial pitch angle and energy.

[47] For a given L^*, bounce averaged diffusion rates are highest between just before local midnight, through dawn to noon MLT, and reflect the higher levels of chorus wave power typically observed in that region. The diffusion rates increase significantly with increasing K_p. The latitude distribution shows that most wave diffusion occurs close to the geomagnetic equator, and that electron diffusion at large equatorial pitch angles must occur near the magnetic equator.

[48] Combining the diffusion rates for a given MLT to form the drift and bounce averaged diffusion rates, we find that electron diffusion by lower band chorus increases with L^* and is very significant at $L^* = 8$ even for low levels of geomagnetic activity (K_p < 1). Pitch angle and energy diffusion extend up to MeV energies, but at high energies, energy diffusion at large pitch angles exceeds pitch angle diffusion at the loss cone indicating that the waves can accelerate electrons with little loss. For moderate and high levels of K_p, lower band chorus also produces significant energy diffusion near 1 keV near the loss cone which may be related to the growth of the waves.

[49] In contrast to lower band chorus, electron diffusion by upper band chorus is restricted to mainly L^* < 6 according to the distribution of wave intensity, but the reason why the waves are restricted is unclear. The combined diffusion rates for upper and lower band chorus result in two maxima in the pitch angle diffusion rates which are most evident at small pitch angles and which are likely to lead to energy-dependent structure in the electron distribution function and the formation of pancake distributions.

[50] The chorus diffusion matrix developed here should provide a valuable resource for use in global models of the radiation belts and for space weather applications to forecast the radiation belt electron flux using physical models that include wave particle interactions [e.g., *Horne et al.*, 2013].

[51] **Acknowledgments.** We thank the NSSDC Omniweb for providing the *Kp* indices used in this paper. The research leading to these results has received funding from the European Union Seventh Framework Programme (FP7/2007-2013) under grant agreements 262468 (SPACECAST) and 284520 (MAARBLE). We also acknowledge financial support from the Natural Environment Research Council and NASA grant NNX11AR64G, and the International Space Science Institute (ISSI), Bern, Switzerland, for 2 one week meetings in 2011 and 2013.

[52] Robert Lysak thanks David Nunn and an anonymous reviewer for their assistance in evaluating this paper.

References

Agapitov, O., A. Artemyev, V. Krasnoselskikh, Y. V. Khotyaintsev, D. Mourenas, H. Breuillard, M. Balikhin, and G. Rolland (2013), Statistics of whistler-mode waves in the outer 1 radiation belt: Cluster STAFF-SA measurements, *J. Geophys. Res. Space Physics*, *118*, 3407–3420, doi:10.1002/jgra.50312.

Albert, J. M., N. P. Meredith, and R. B. Horne (2009), Three-dimensional diffusion simulation of outer radiation belt electrons during the October 9, 1990, magnetic storm, *J. Geophys. Res.*, *114*, A09214, doi:10.1029/2009JA014336.

Baker, D. N., S. G. Kanekal, X. Li, S. P. Monk, J. Goldstein, and J. L. Burch (2004), An extreme distortion of the Van Allen belt arising from the ‘Hallowe’en’ solar storm in 2003, *Nature*, *432*, 878–881.

Boscher, D., S. Bourdarie, P. O’Brien, and T. Guild (2008), ONERA-DESP library V4.2. Toulouse-France, 2004-2008.

Breneman, A. W., C. A. Kletzing, J. Pickett, J. Chum, and O. Santolik (2009), Statistics of multispacecraft observations of chorus dispersion and source location, *J. Geophys. Res.*, *114*, A06202, doi:10.1029/2008JA013549.

Burtis, W. J., and R. A. Helliwell (1969), Banded chorus—A new type of VLF radiation observed in the magnetosphere by OGO 1 and OGO 3, *J. Geophys. Res.*, *74*(11), 3002–3010.

Burton, R. K., and R. E. Holzer (1974), The origin and propagation of chorus in the outer magnetosphere, *J. Geophys. Res.*, *79*, 1014–1023.

Carpenter, D. L., and R. R. Anderson (1992), An ISEE/whistler model of equatorial electron density in the magnetosphere, *J. Geophys. Res.*, *97*, 1097–1108.

Cattell, C., et al. (2008), Discovery of very large amplitude whistler-mode waves in Earth’s radiation belts, *Geophys. Res. Lett.*, *35*, L01105, doi:10.1029/2007GL032009.

Chen, Y., G. D. Reeves, and R. H. W. Friedel (2007), The energization of relativistic electrons in the outer Van Allen radiation belt, *Nat. Phys.*, *3*, 614–617.

Fok, M.-C., R. B. Horne, N. P. Meredith, and S. A. Glauert (2008), Radiation Belt Environment model: Application to space weather nowcasting, *J. Geophys. Res.*, *113*, A03S08, doi:10.1029/2007JA012558.

Furuya, N., Y. Omura, and D. Summers (2008), Relativistic turning acceleration of radiation belt electrons by whistler mode chorus, *J. Geophys. Res.*, *113*, A04224, doi:10.1029/2007JA012478.

Glauert, S. A., and R. B. Horne (2005), Calculation of pitch angle and energy diffusion coefficients with the PADIE code, *J. Geophys. Res.*, *110*, A04206, doi:10.1029/2004JA010851.

Goldstein, B. E., and B. T. Tsurutani (1984), Wave normal directions of chorus near the equatorial source region, *J. Geophys. Res.*, *89*, 2789–2810.

Green, J. C., and M. G. Kivelson (2004), Relativistic electrons in the outer radiation belt: Differentiating between acceleration mechanisms, *J. Geophys. Res.*, *109*, A03213, doi:10.1029/2003JA010153.

Gurnett, D. A., and F. L. Scarf (1983), Plasma waves in the Jovian magnetosphere, in *Physics of the Jovian Magnetosphere*, edited by A. J. Dessler, pp. 285–316, Cambridge University Press, Cambridge.

Gurnett, D. A., W. S. Kurth, F. L. Scarf, and R. L. Poynter (1986), First plasma wave observations at Uranus, *Science*, *233*, 106–109.

Haque, N., M. Spasojevic, O. Santolk, and U. S. Inan (2010), Wave normal angles of magnetospheric chorus emissions observed on the Polar spacecraft, *J. Geophys. Res.*, *115*, A00F07, doi:10.1029/2009JA014717.

Hayakawa, M., Y. Yamanaka, M. Parrot, and F. Lefeuvre (1984), The wave normals of magnetospheric chorus emissions observed on board GEOS 2, *J. Geophys. Res.*, *89*, 2811–2821.

Horne, R. B., and R. M. Thorne (1998), Potential waves for relativistic electron scattering and stochastic acceleration during magnetic storms, *Geophys. Res. Lett.*, *25*, 3011–3014.

Horne, R. B., and R. M. Thorne (2003), Relativistic electron acceleration and precipitation during resonant interactions with whistler-mode chorus, *Geophys. Res. Lett.*, *30*(10), 1527, doi:10.1029/2003GL0169731.

Horne, R. B., S. A. Glauert, and R. M. Thorne (2003), Resonant diffusion of radiation belt electrons by whistler-mode chorus, *Geophys. Res. Lett.*, *30*(9), 1493, doi:10.1029/2003GL016963.

Horne, R. B., R. M. Thorne, Y. Y. Shprits, N. P. Meredith, S. A. Glauert, A. J. Smith, S. G. Kanekal, D. N. Baker, M. J. Engebretson, J. L. Posch, M. Spasojevic, U. S. Inan, J. S. Pickett, and P. M. E. Decreau (2005a), Wave acceleration of electrons in the Van Allen radiation belts, *Nature*, *437*, 227–230, doi:10.1038/nature03939.

Horne, R. B., R. M. Thorne, S. A. Glauert, J. M. Albert, N. P. Meredith, and R. R. Anderson (2005b), Timescale for radiation belt electron acceleration by whistler mode chorus waves, *J. Geophys. Res.*, *110*, A03225, doi:10.1029/2004JA010811.

Horne, R. B. (2007), Plasma astrophysics: Acceleration of killer electrons, *Nat. Phys.*, *3*, 590–591.

Horne, R. B., R. M. Thorne, S. A. Glauert, J. D. Menietti, Y. Y. Shprits, and D. A. Gurnett (2008), Gyro-resonant electron acceleration at Jupiter, *Nat. Phys.*, *4*, 301–304, doi:10.1038/nphys897.

Horne, R. B., S. A. Glauert, N. P. Meredith, D. Heynderickx, D. Boscher, V. Maget, and D. Pitchford (2013), Space Weather effects on satellites and forecasting the Earth's electron radiation belts with SPACECAST, *Space Weather*, *11*, doi:10.1002/swe.20023.

Hospodarsky, G. B., T. F. Averkamp, W. S. Kurth, D. A. Gurnett, J. D. Menietti, O. Santolik, and M. K. Dougherty (2008), Observations of chorus at Saturn using the Cassini Radio and Plasma Wave Science instrument, *J. Geophys. Res.*, *113*, A12206, doi:10.1029/2008JA013237.

Imhof, W. L., H. D. Voss, J. Mobilia, D. W. Datlowe, E. E. Gaines, J. P. McGlennon, and U. S. Inan (1992), Relativistic electron microbursts, *J. Geophys. Res.*, *97*, 13,829–13,837.

Jordanova, V. K., R. M. Thorne, W. Li, and Y. Miyoshi (2010), Excitation of whistler mode chorus from global ring current simulations, *J. Geophys. Res.*, *115*, A00F10, doi:10.1029/2009JA014810.

Katoh, Y., and Y. Omura (2007), Computer simulation of chorus wave generation in the Earth's inner magnetosphere, *Geophys. Res. Lett.*, *34*, L03102, doi:10.1029/2006GL028594.

Katoh, Y., and Y. Omura (2011), Amplitude dependence of frequency sweep rates of whistler mode chorus emissions, *J. Geophys. Res.*, *116*, A07201, doi:10.1029/2011JA016496.

Kennel, C. F., and H. E. Petschek (1966), Limit on stably trapped particle fluxes, *J. Geophys. Res.*, *71*, 1–28.

Lauben, D. S., U. S. Inan, T. F. Bell, and D. A. Gurnett (2002), Source characteristics of ELF/VLF chorus, *J. Geophys. Res.*, *107*(A12), 1429, doi:10.1029/2000JA003019.

Li, W., Y. Y. Shprits, and R. M. Thorne (2007), Dynamic evolution of energetic outer zone electrons due to wave-particler interactions during storms, *J. Geophys. Res.*, *112*, A10220, doi:10.1029/2007JA012368.

Li, W., R. M. Thorne, V. Angelopoulos, J. Bortnik, C. M. Cully, B. Ni, O. LeContel, A. Roux, U. Auster, and W. Magnes (2009), Global distribution of whistler-mode chorus waves observed on the THEMIS spacecraft, *Geophys. Res. Lett.*, *36*, L09104, doi:10.1029/2009GL037595.

Li, W., R. M. Thorne, J. Bortnik, Y. Nishimura, V. Angelopoulos, L. Chen, J. P. McFadden, and J. W. Bonnell (2010), Global distributions of suprathermal electrons observed on THEMIS and potential mechanisms for access into the plasmasphere, *J. Geophys. Res.*, *115*, A00J10, doi:10.1029/2010JA015687.

Li, W., J. Bortnik, R. M. Thorne, and V. Angelopoulos (2011), Global distribution of wave amplitudes and wave normal angles of chorus waves using THEMIS wave observations, *J. Geophys. Res.*, *116*, A12205, doi:10.1029/2011JA017035.

Li, W., R. M. Thorne, J. Bortnik, R. McPherron, Y. Nishimura, V. Angelopoulos, and I. G. Richardson (2012), Evolution of chorus waves and their source electrons during storms driven by corotating interaction regions, *J. Geophys. Res.*, *117*, A08209, doi:10.1029/2012JA017797.

Lyons, L. R., D.-Y. Lee, R. M. Thorne, R. B. Horne, and A. J. Smith (2005), Solar-wind magnetosphere coupling leading to relativistic electron energization during high-speed streams, *J. Geophys. Res.*, *110*, A11202, doi:10.1029/2005JA011254.

Lorentzen, K. R., J. B. Blake, U. S. Inan, and J. Bortnik (2001), Observations of relativistic electron microbursts in association with VLF chorus, *J. Geophys. Res.*, *106*, 6017–6027.

Markwardt, C. B. (2009), Non-linear least squares fitting in IDL with MPFIT, in *Proc. Astronomical Data Analysis Software and Systems XVIII, Quebec, Canada, ASP Conference Series*, edited by D. Bohlender, P. Dowler, and D. Durand, vol. 411, pp. 251–254, Astronomical Society of the Pacific, San Francisco, Calif.

Meredith, N. P., A. D. Johnstone, R. B. Horne, and R. R. Anderson (2000), The temporal evolution of injected electron distributions in the inner magnetosphere, *J. Geophys. Res.*, *105*, 12,907–12,917.

Meredith, N. P., R. B. Horne, and R. R. Anderson (2001), Substorm dependence of chorus amplitudes: Implications for the acceleration of electrons to relativistic energies, *J. Geophys. Res.*, *106*, 13,165–13,178.

Meredith, N. P., R. B. Horne, D. Summers, R. M. Thorne, R. H. A. Iles, D. Heynderickx, and R. R. Anderson (2002), Evidence for acceleration of outer zone electrons to relativistic energies by whistler mode chorus, *Ann. Geophys.*, *20*, 967–979.

Meredith, N. P., R. B. Horne, R. M. Thorne, and R. R. Anderson (2003), Favored regions for chorus-driven electron acceleration to relativistic energies in the Earth's outer radiation belt, *Geophys. Res. Lett.*, *30*(16), 1871, doi:10.1029/2003GL017698.

Meredith, N. P., R. B. Horne, R. M. Thorne, D. Summers, and R. R. Anderson (2004), Substorm dependence of plasmaspheric hiss, *J. Geophys. Res.*, *109*, A06209, doi:10.1029/2004JA010387.

Meredith, N. P., R. B. Horne, A. Sicard-Piet, D. Boscher, K. H. Yearby, W. Li, and R. M. Thorne (2012), Global model of lower band and upper band chorus from multiple satellite observations, *J. Geophys. Res.*, *117*, A10225, doi:10.1029/2012JA017978.

Miyoshi, Y., A. Morioka, R. Kataoka, Y. Kasahara, and T. Mukai (2007), Evolution of the outer radiation belt during the November 1993 storms driven by corotating interaction regions, *J. Geophys. Res.*, *112*, A05210, doi:10.1029/2006JA012148.

Miyoshi, Y., Y. Katoh, T. Nishiyama, T. Sakanoi, K. Asamura, and M. Hirahara (2010), Time of flight analysis of pulsating aurora electrons, considering wave-particle interactions with propagating whistler mode waves, *J. Geophys. Res.*, *115*, A10312, doi:10.1029/2009JA015127.

Muto, H., M. Hayakawa, M. Parrot, and F. Leveuvre (1987), Direction finding of half-gyrofrequency VLF emissions in the off-equatorial region of the magnetosphere and their generation and propagation, *J. Geophys. Res.*, *92*, 7538–7550.

Ni, B., R. M. Thorne, N. P. Meredith, R. B. Horne, and Y. Y. Shprits (2011), Resonant scattering of plasma sheet electrons leading to diffuse auroral precipitation: 2. Evaluation for whistler mode chorus waves, *J. Geophys. Res.*, *116*, A04219, doi:10.1029/2010JA016233.

Nishimura, Y., et al. (2010), Identifying the driver of the pulsating aurora, *Science*, *330*, 81–84, doi:10.1126/science.1193186.

Nunn, D. (1974), A self-consistent theory of triggered VLF emissions, *Planet. Space Sci.*, *22*, 349–378.

Nunn, D., Y. Omura, H. Matsumoto, I. Nagano, and S. Yagitani (1997), The numerical simulation of VLF chorus and discrete emissions observed on the Geotail satellite using a Vlasov code, *J. Geophys. Res.*, *102*(A12), 27,083–27,097.

Nunn, D., O. Santolik, M. Rycroft, and V. Trakhtengerts (2009), On the numerical modelling of VLF chorus dynamical spectra, *Ann. Geophys.*, *27*(27), 2341–2359.

Olson, W. P., and K. Pfitzer (1977), Magnetospheric magnetic field modeling. Annual Scientific Report, AFOSAR Contract No. F44620-75-c-0033.

Omura, Y., D. Nunn, H. Matsumoto, and M. J. Rycroft (1991), A review of observational, theoretical and numerical studies of VLF triggered emissions, *J. Atmos. Terr. Phys.*, *53*, 351–368.

Omura, Y., N. Furuya, and D. Summers (2007), Relativistic turning acceleration of resonant electrons by coherent whistler mode waves in a dipole magnetic field, *J. Geophys. Res.*, *112*, A06236, doi:10.1029/2006JA012243.

Omura, Y., M. Hikishima, Y. Katoh, D. Summers, and S. Yagitani (2009), Nonlinear mechanisms of lower-band and upper-band VLF chorus emissions in the magnetosphere, *J. Geophys. Res.*, *114*, A07217, doi:10.1029/2009JA014206.

Rosenberg, T. J., R. A. Helliwell, and J. P. Katsufrakis (1971), Electron precipitation associated with discrete very-low-frequency emissions, *J. Geophys. Res.*, *76*, 8445–8452.

Saito, S., Y. Miyoshi, and K. Seki (2012), Relativistic electron microbursts associated with whistler chorus rising tone elements: GEMSIS-RBW simulations, *J. Geophys. Res.*, *117*, A10206, doi:10.1029/2012JA018020.

Santolík, O., D. A. Gurnett, and J. S. Pickett (2003), Spatio-temporal structure of storm-time chorus, *J. Geophys. Res.*, *108*(A7), 1278, doi:10.1029/2002JA009791.

Santolík, O., J. S. Pickett, D. A. Gurnett, J. D. Menietti, B. T. Tsurutani, and O. Verkhoglyadova (2010), Survey of Poynting flux of whistler mode chorus in the outer zone, *J. Geophys. Res.*, *115*, A00F13, doi:10.1029/2009JA014925.

Scarf, F. L., D. A. Gurnett, W. S. Kurth, F. V. Coroniti, C. F. Kennel, and R. L. Poynter (1987), Plasma wave measurements in the magnetosphere of Uranus, *J. Geophys. Res.*, *92*(A13), 15,217–15,224.

Schulz, M., and L. Lanzerotti (1974), *Particle Diffusion in the Radiation Belts*, Springer, New York.

Shprits, Y. Y., L. Chen, and R. M. Thorne (2009a), Simulations of pitch angle scattering of relativistic electrons with MLT-dependent diffusion coefficients, *J. Geophys. Res.*, *114*, A03219, doi:10.1029/2008JA013695.

Shprits, Y. Y., D. Subbotin, and B. Ni (2009b), Evolution of electron fluxes in the outer radiation belt computed with the VERB code, *J. Geophys. Res.*, *114*, A11209, doi:10.1029/2008JA013784.

Shue, J. H., J. K. Chaoa, H. C. Fu, C. T. Russell, P. Song, K. K. Khurana, and H. J. Singer (1997), A new functional form to study the solar wind control of the magnetopause size and shape, *J. Geophys. Res.*, *102*(A5), 9497–9511.

Shue, J. H., P. Song, C. T. Russell, J. T. Steinberg, J. K. Chaoa, G. Zastenker, O. L. Vaisberg, S. Kokubun, H. J. Singer, T. R. Detman, and H. Kawano (1998), Magnetopause location under extreme solar wind conditions, *J. Geophys. Res.*, *103*(A8), 17,691–17,700.

Smith, A. J., R. B. Horne, and N. P. Meredith (2004a), Ground observations of chorus following geomagnetic storms, *J. Geophys. Res.*, *109*, A02205, doi:10.1029/2003JA010204.

Smith, A. J., N. P. Meredith, and T. P. O'Brien (2004b), Differences in ground-observed chorus in geomagnetic storms with and without enhanced relativistic electron fluxes, *J. Geophys. Res.*, *109*, A11204, doi:10.1029/2004JA010491.

Su, Z., F. Xiao, H. Zheng, and S. Wang (2010), STEERB: A three-dimensional code for storm-time evolution of electron radiation belt, *J. Geophys. Res.*, *115*, A09208, doi:10.1029/2009JA015210.

Summers, D., R. M. Thorne, and F. Xiao (1998), Relativistic theory of wave-particle resonant diffusion with application to electron acceleration in the magnetosphere, *J. Geophys. Res.*, *103*(20), 20,487–20,500.

Tao, X., R. M. Thorne, W. Li, B. Ni, N. P. Meredith, and R. B. Horne (2011), Evolution of electron pitch angle distributions following injection from the plasma sheet, *J. Geophys. Res.*, *116*, A04229, doi:10.1029/2010JA016245.

Thorne, R. M., B. Ni, X. Tao, R. B. Horne, and N. P. Meredith (2010), Scattering by chorus waves as the dominant cause of diffuse auroral precipitation, *Nature*, *467*, 943–946, doi:10.1038/nature09467.

Trakhtengerts, V. Y. (1999), A generation mechanism for chorus emission, *Ann. Geophys.*, *17*, 95–100.

Tsurutani, B. T., and E. J. Smith (1974), Postmidnight chorus: A substorm phenomenon, *J. Geophys. Res.*, *79*, 118–127.

Tsurutani, B. T., and E. J. Smith (1977), Two types of magnetospheric ELF chorus and their substorm dependencies, *J. Geophys. Res.*, *82*, 5112.

Tsurutani, B. T., G. S. Lakhina, and O. P. Verkhoglyadova (2013), Energetic electron (> 10 keV) microburst precipitation, 5–15 s X-ray pulsations, chorus and wave-particle interactions: A review, *J. Geophys. Res. Space Physics*, *118*, 2296–2312, doi:10.1002/jgra.50264.

Varotsou, A., D. Boscher, S. Bourdarie, R. B. Horne, S. A. Glauert, and N. P. Meredith (2005), Simulation of the outer radiation belt electrons near geosynchronous orbit including both radial diffusion and resonant interaction with whistler-mode chorus waves, *Geophys. Res. Lett.*, *32*, L19106, doi:10.1029/2005GL023282.

Varotsou, A., D. Boscher, S. Bourdarie, R. B. Horne, N. P. Meredith, S. A. Glauert, and R. H. Friedel (2008), Three-dimensional test simulations of the outer radiation belt electron dynamics including electron-chorus resonant interactions, *J. Geophys. Res.*, *113*, A12212, doi:10.1029/2007JA012862.